Delft University of Technology
Master's Thesis in Embedded Systems

Computational Imaging for Earth Surveillance

Pranav Sailesh Mani

Computational Imaging for Earth Surveillance

Master's Thesis in Embedded Systems

Embedded Software Section
Faculty of Electrical Engineering, Mathematics and Computer Science
Delft University of Technology
Mekelweg 4, 2628 CD Delft, The Netherlands

Pranav Sailesh Mani
p.s.mani@student.tudelft.nl

26th August 2017

Author

Pranav Sailesh Mani (p.s.mani@student.tudelft.nl)

Title

Computational Imaging for Earth Surveillance

MSc presentation

26th August 2017

Graduation Committee

TODO GRADUATION COMMITTEE	Delft University of Technology
TODO GRADUATION COMMITTEE	Delft University of Technology

Abstract

TODO ABSTRACT

Preface

TODO MOTIVATION FOR RESEARCH TOPIC

TODO ACKNOWLEDGEMENTS

TODO AUTHOR

Delft, The Netherlands
26th August 2017

Contents

Chapter 1

Introduction and Problem Statement

The history of cameras go back to 13th century when Aristotle first noticed how light passing through a small hole in a darkened room produced an image of the sun on the wall. Throughout the centuries, the basic design of cameras have been continuously changing with different versions of the 'camera obscura'. 'Camera Obscura' is a phenomenon that occurs when when a scene is projected onto a pinhole and the image of that scene is formed on the surface opposite to that of a pinhole.

In a pinhole camera, light passes through the pinhole and forms an image on the sensor/image plane.As the size of the pinhole increased, the quality of image formed on the plane decreased and as the pinhole size became smaller, lesser light was allowed which resulted in decreased field of view. With the development of science and due to the limitations of the pinhole, lenses were introduced to increase the size of the aperture, the sharpness of the image and the light throughput. As humanity progressed with the rapid pace in technology, we were able to capture images and store them on a film. With the digital explosion in early 1990s, the thin films were replaced by Charged Couple Devices(CCD). Then came the cameras based on Complementary Metal Oxide Semiconductors(CMOS). CCD and CMOS sensors reduced the size of cameras considerably and it was possible to develop low cost cameras in a large number. However, cameras have retained the lens throughout the years. Cameras are used for various applications and one such application is the space exploration domain.

Delfi Space is the small satellite program of TU Delft that is mainly meant for education and technology demonstration in very small sized satellites. Delfi-PQ programme is a sub-programme of the Delfi Space programme that aims at developing extremely small but highly capable PocketQube satellites. PocketQubes are an order of magnitude smaller than the well known CubeSat standard which formed the basis of previous Delfi satellite projects. The dimensions of a PocketQube satellite would be 50mm * 50mm * 178mm and their volume would be approximately eight times smaller than CubeSats. One of the advanced payload that would be part of the Delfi-PQ would be an imager/camera that consumes extremely low power and would fit into the dimensions specified by the Delfi-PQ team. The thickness of the camera should be less than 6mm thick.

In order to reduce the size of a camera, it would be necessary to remove the lens from the camera as the thinnest lens based mobile camera is 5mm thick. The primary focus of a lens would be to focus light from distant objects onto the CMOS sensor. Light from distant objects reach the sensor even without the lens except that the light is incoherent and the CMOS sensor would not be able to form the object properly without a lens. However, the lens could also be replaced by coded apertures. Coded Apertures have been used in the late 20th century to image X-Ray sources of light. Lensless coded aperture cameras can be as small as $100\mu m$ thick. By using lensless cameras, we could potentially reduce the form-facto multiple times to suit the requirements of Delfi-PQ. This thesis would address the following research question:

Is it possible to design “lensless coded” aperture cameras with a small form-factor(thickness < 10mm) using COTS(commercial off-the-shelf) components that can be used in U-class Spacecrafts ?

This question can be broken down into the following sub-questions:

- Would it be possible to design a lensless camera to capture astronomical objects in the visible range of light spectrum?
- What would be the minimum possible form-factor that would be achievable and the effects of different factors such as diffraction effects, mask-to-sensor distance and reconstruction algorithms?
- If possible, how would the lensless camera compare with the conventional lens based cameras used currently?
- Would it be possible to design a lensless camera that would fit the size constraints of the Delfi-PQ?

Chapter 2

Literature Survey and Trade-off Analysis

In this chapter, a state-of-the art study will be presented that could assist in design of the lensless imager with specifications mentioned in the previous chapter.

2.1 Camera Computational Pipeline

In order to design a lensless imaging system, we must first look at the computational imaging pipeline of existing cameras. Since the lensless camera basically uses computation to reconstruct images, it is important to understand the computational pipeline of existing camera systems and make necessary modification in the design of the existing pipeline to suit the system. The computational imaging pipeline of existing camera systems is shown figure 2.1[8]. As shown in figure 2.1, there are five main components that can be controlled computationally in existing systems. Illumination of the scene can be controlled to produce an enhanced picture. Optics could be controlled to limit the amount of light entering the scene and thereby controlling the image produced on the sensor. The sensor can also computationally modify the date it receives to de-noise, adjust the blackness/white

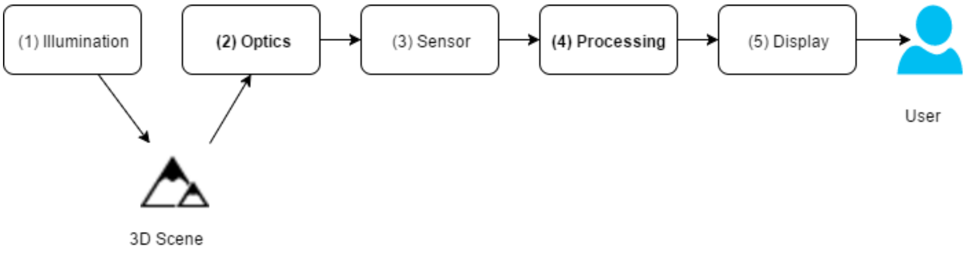

Figure 2.1: Computational Pipeline of Existing cameras

in an image. Post-processing can also be done on the image produced by the sensor to improve the image produced by the sensor. Finally, a display can also be modified computationally to produce certain effects on the user. And of course, the user can control any of these components to produce the effect he desires. But in the case of the lensless imaging system, we would be modifying the optics and the processing components of the pipeline to reduce the size of the camera.The components to be modified are are darkened in figure 2.1.

2.2 Satellite Imaging Architectures

Since the camera is going to be capturing pictures of the earth, it would be required to study the existing imaging architectures currently being used in satellites and how the design of the lensless camera would fit into the existing imaging architectures. We will first look into the terminology commonly used in space instrumentation. As the imager is carried along the orbit of the earth, it images a strip on the surface of the earth. The width of the strip is called the 'swath'. The direction along which the satellite moves or images is called the 'along-track' direction and the direction perpendicular to it is called the cross-track direction[1]. Figure 2.2 describes these terminology and some other terms as well. Three major types of scanning architectures

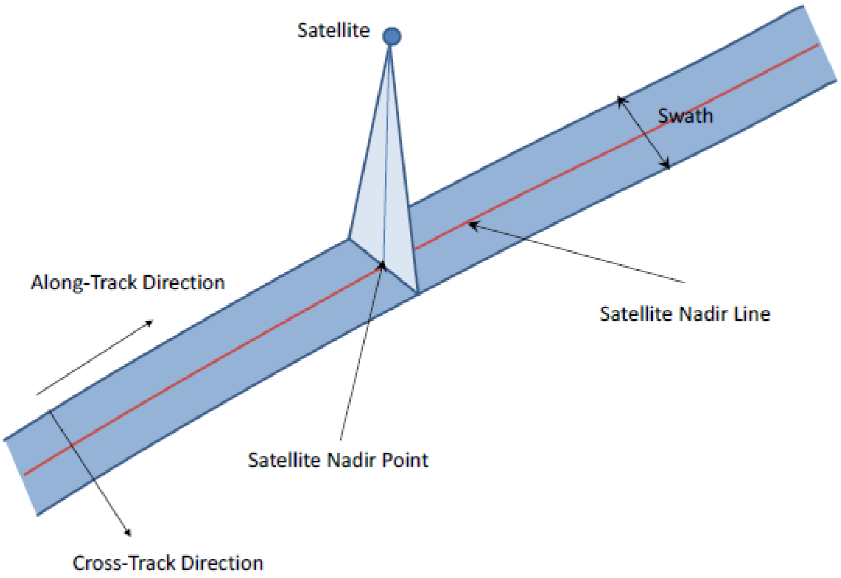

Figure 2.2: Various Imaging Terms[1]

are employed in space instruments, namely:

- Whiskbroom Line Scanner: In this type of scanning architecture, a detector element detects it's instantaneous field of view which is projected onto a pixel element. In this scanning type the surface of the earth is scanned in lines. A scanning mirror would project a very small area of the earth onto the single pixel element. The scanning mirror would then rotate to project the next element of the line onto the next pixel. Depending on the motion of the satellite, the next line of the detector is scanned and projected on to the next line on the surface of the earth. An advantage of this type of detector is that it would be possible to obtain a very large field of view. However, it also comes with disadvantage that a very high sampling frequency is required to get decent resolutions. Typically, an earth observation satellite would move at 6.5 km per second. In order to get a resolution of 100 meters per pixel, it would be required to sample atleast 65 lines per second. For a swath of 1000 pixels it would be required to sample at 65000 elements per second. Apart from this, there is very limited time for each detector element which would result in low spatial resolution[10]. Another main disadvantage is that mechanical components would be required to project different parts of the surface of the earth on to the detector element. This type of scanner is also called as along-track scanner. Mathematically, the measurement of the detector element (X, Y) can be described using

  $$(X, Y) = f(t_x, t_y)$$

  where t_x and t_y is the time at which the image is captured in the corresponding location

- Pushbroom Line Scanner : In this type of architecture, the orbital motion of the sensor is used to image the swath instead of using a mirror as in the case of whiskbroom scanner. The field of view in the cross-track direction is imaged by the corresponding line detector array. Successive lines are imaged and sampled by the multiplexer as the sensor moves across the surface. The time between sampling two successive lines can be the time it takes for the satellite to move that distance. The most commonly used detector for a pushbroom scanner is Charge Coupled Devices(CCD). One of the main advantages of this type of scanner is that it requires no moving parts. Due to this, it is possible to obtain very high scanning rates(¡ 1μ second). This also leads to lower noise in the received signal[10]. The disadvantage is that large number of detectors are required to image a large piece of area. In addition to this, it requires an optical arrangement that could obtain a wide field of view. Mathematically, the measurement of the detector element (X, Y) can be described using

  $$(X, Y) = f(x), f(t_y)$$

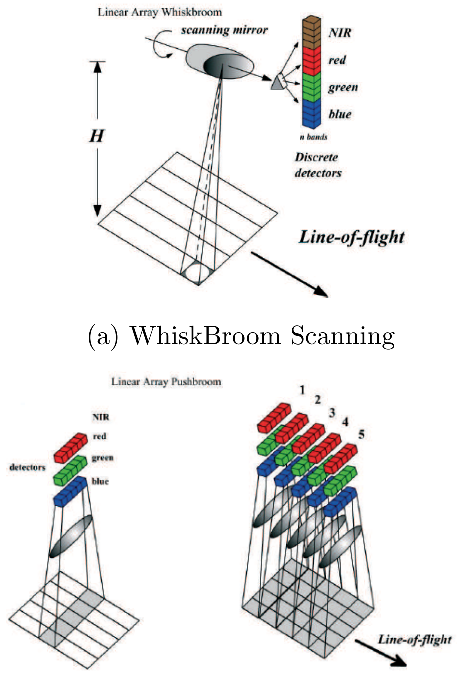

(a) WhiskBroom Scanning

(b) Pushbroom Scanning

Figure 2.3: A figure with two subfigures

where $f(x)$ represents the sensor output and $f(t_y)$ represents the time at which the subsequent rows are imaged.

- Staring Array : Staring arrays use 2-d CCD/CMOS detectors to capture an entire area on the surface of the earth. These are also called as framing cameras. This provides speed-up and step-and-stare mechanism is employed wherein observations are made intermittently after a certain number of steps in the cross-track direction. The advantage is that moderate field of view optics is only required in this case[10]. Mathematically, the measurement of the detector element (X, Y) can be described using

$$(X, Y) = f(x), f(y)$$

where $f(x)$ and $f(y)$ represents the sensor output.

2.3 Trade-off Analysis

2.3.1 Camera Sensor

The camera sensor is the core of the Delfi-PQ Imager. The performance of a camera is mainly limited by the image sensor that it uses[9]. The camera sensor can be off two types namely, CCD(charge coupled device) or CMOS(Complimentary Metal Oxide Semiconductor). Both the types of CMOS sensors have their own advantages and disadvantages. To understand the challenges that each type of sensor poses, we must understand how the sensors are designed.

The following factors have been chosen to make a trade-off between the different CMOS sensors:

1. Resolution : When rating a camera, the first thing that comes to the mind is the resolution of the camera. The resolution of a camera is directly dependent on the number of pixels in the image sensor of the camera.

2. Power Consumption : In the design of the PQ-Camera, the most important factor is the power consumption of the entire imager. The majority of the power consumption by the imager is dependent on the power consumption of the CMOS sensor.

3. Availability : Even though there are innumerable number of CMOS sensors in the world, availability of CMOS sensors is quite low when it comes to small-scale. Many CMOS manufacturers require large scale orders.

4. Quantum Efficiency(QE) : Quantum Efficiency is the measure of efficiency of the camera sensor to convert incoming photons into electrons. The ratio of electrons generated during the digitization process to photons is called quantum efficiency.

5. Pixel Size : Pixel size is the size of each pixel unit in the CMOS camera. It is also an important factor considering that the signal produced by the CMOS sensor depends on the pixel size as well.

$$Signal = LightDensity * (PixelSize)^2 * QE$$

6. Electronic Interface : The electronic interface that can be used to retreive data from the CMOS sensor also plays an important role. Since the project uses a low-power microcontroller that has limited communication capabilities, it would be wise to chose an interface that is supported by the microcontroller. Recently available chips use LVDS/MIPI interface to send data. These interfaces are not supported by the microcontroller that is being used as an on-board computer. The on-board computer uses an I2C based interface and that the electronic interface would be an important factor as it would reduce the complexity of the system and also reduce the power consumption by removing the addidional circuitry necessary for interfacing with the onboard computer.

7. Dynamic Range : Dynamic Range and SNR are used interchangeably in CMOS sensors. The only difference is that dynamic range considers only the temporal dark noise while SNR includes the root mean square of the shot noise as well.

8. Shutter Type : Camera sensors use different types of shutters namely, global shutter and rolling shutter. Global shutter reduces the distortions due to fast moving artefacts while increasing the dark current. Rolling shutter has more distortions in the case of imaging moving artefacts, but also has lesser dark noise compared to global shutter.

9. Voltage Level : Voltage level also has to be taken into account while choosing the sensor because if the CMOS sensor needs a voltage level higher than that of the main satellite bus voltage, then additional circuitry has to be introduced to step up the voltage level which in turn increases the overall system power.

10. Operating Temperature : Operating temperature is an important factor to take into account when choosing an imaging sensor. Since the camera is going to operate in space, it is better if the CMOS sensor has a higher operating range of temperature.

11. Overall Size and Weight : As the imager has to fit within specific dimensions, the overall size and weight of the CMOS sensor also needs to be taken into account.

12. Frame Rate: Even though, it is not required to have a camera sensor that is capable of high frame rates, it is an added advantage and higher frame rate camera could help in imaging larger areas of the earth if required.

13. Price: While there are no specific cost constraints in the project, price has also been taken into account.

In [11], a survey of camera modules for a CubeSat space Mission has already been carried. However, we also consider image sensors(not same as camera modules) as we are fundamentally changing the design of a camera.

The following candidates have been chosen for analysis. These candidates are chosen based on [11] and also on the latest CMOS sensors available on the market.

(a) IDS UI- 1646LE USB 1.3MP

(b) C3188A

(c) PC67XC-2 CCD

(d) MicroCam TTL

(e) PB-MV40

(f) Omnivision OV7670

(g) Sony ICX285AL

(h) Omnivision OV5642

(i) Omnivision OV2740

(j) MCM20027

Table 2.1: Comparison of Different Image Sensor Candidates

Candidates Factors	(a)	(b)	(c)	(d)	(e)	(f)	(g)	(h)	(i)	(j)
Optical Parameters										
Resolution	++	+	+	-	++	+	++	++	++	++
Pixel Size	+	++	X	++	++	+	++	+	+	++
Shutter type	-	-	X	-	-	+	+	+	+	-
Frame Rate	+	+	+	+	+++	+	+	+	+	+
Electrical and other parameters										
Power Consumption	- -	- -	- - -	++	-	++	-	- - -	- -	- -
Availability	-	+	- - -	- - -	- - -	++	- -	++	- -	- - -
Electronic Interface	+	+	- - -	++	- -	++	- -	++	-	+
DR and SNR	X	+	X	++	+	++	+	++	+	+
Voltage	+	+	- - -	++	+	++	+	++	-	+
Operating Temperature	+	+	+	+	+	+	+	+	+	+
Overall Size and Weight	+	+	+	+	+	+	+	+	+	+
Price	-	+	X	X	- - -	++	X	+	X	X
Points	2	8	-8	8	0	18	5	13	2	4

2.3.2 Compression Algorithms

2.3.3 Reconstruction Algorithms

The simplest lensless imaging system is the pinhole camera. However, since the quality of the image depends on the size of the pinhole, that restricts the amount of light that can enter the imaging system. Lenses were introduced to focus the light from distant objects onto a film or a sensor. In the absense of a lens, the sensor would record the average intensity of the light entering it. This can also bee seen in the experiments which are described in the upcoming chapters. Coded aperture cameras extend the pinhole camera concept replacing the single aperture with a mask containing multiple apertures. The first developed coded aperture cameras were used in imaging X-Ray sources due to the difficulty involved in focussing light from X-Ray sources[6]. Since a single pinhole limits the amount of light imaged by the sensing element, it was replaced by many holes, called the aperture so that overlapping images are formed on the film. The recorded image will have no similarity with the source and an digital processing is required to reconstruct the source image or the object. The recorded image is mathematically modelled as a collection of overlapping shadows as described by the following equation[5][6]

$$y = \phi * x + e \tag{2.1}$$

where y represents the image formed on the sensor, ϕ represents the mask pattern, x represents the irradiance vector or the object and e represents the noise. The $*$ operator represents the convolution operation between the mask an the object. The coded aperture increases the flux that falls on the detector and this leads to an increase in the SNR. The SNR can be as large $\sqrt{N}$, where N represents the number of holes in the aperture[6]. The increased SNR comes at the cost of computational decoding for the image.

Chapter 3

System Modelling and Design

This chapter will describe how the system can be mathematically modelled and how the mask for the lensless imager was designed. As mentioned in the previous chapter the system can be modelled as

$$y = \phi * x + e; \tag{3.1}$$

Ignoring the noise and converting the equation to fourier domain, the equation 3.1 can be re-written as

$$F(y) = F(\phi)F(x) \tag{3.2}$$

$$F(x) = \frac{F(y)}{F(\phi)} \tag{3.3}$$

Equation 3.3 is the simplest possible computational inversion of the scene from the sensor. This method has also been used in [7]. As mentioned in the previous chapter, there are two types of masks that can be used for the purpose of encoding the scene onto the mask, namely separable and non-separable mask. MATLAB has been used for the purpose of simulating the algorithms.

3.1 Simulation of a non-separable mask

3.2 Simulation of a separable mask

Chapter 4

Implementation

4.1 Embedded Software of Camera

One of the main reasons behind choosing the OV2640 CMOS sensor is that it has a ready electronic interface that can be used t interface with standard 8-bit/16-bit microcontrollers, The OV2640 is one of the sensors that is available as a part of Arducam hardware. Arducam is an open source camera that comes along with open-source hardware and software that is needed to capture images using the CMOS sensor. However, using the camera comes with its own advantages and disadvantages. The main advantage behind using this platform is that the platform has open-source libraries that could be used to interface with ATMEGA328P, an 8-bit microcontroller. In space-missions, it would not be possible to send high-powered microprocessors, and microcontroller is used as an on-board computer. Arducam has standard software libraries that can be used to interface with Arduino making the cumbersome and lengthy job of writing an interface software to a CMOS sensor way more easier. A disadvantage of the hardware module is the on-board memory that it has to capture an image. The OV2640 Arducam mini camera module can capture upto 1600*1200 resolution images with or without any form of compression. However due to the limitation of the on-board OV2640 FIFO memory AL422B it would be possible to capture only compressed images and not full resolution RAW images. The AL422B on-board FIFO has only 384KB of memory and that is not enough to obtain a full-resolution RAW image. However, we would like to have the RAW unprocessed image from the sensor. One of the other disadvantages is that custom code needs to be written to obtain various controls that we need for our camera. We have to write our own camera control software if we need to control factors such as exposure time, ISO, etc. as the default software uses automatic exposure control to enhance the image quality. The camera module architecture is shown in Figure 4.1.

The system for experiments is as shown in Figure 4.2. The Arduino is

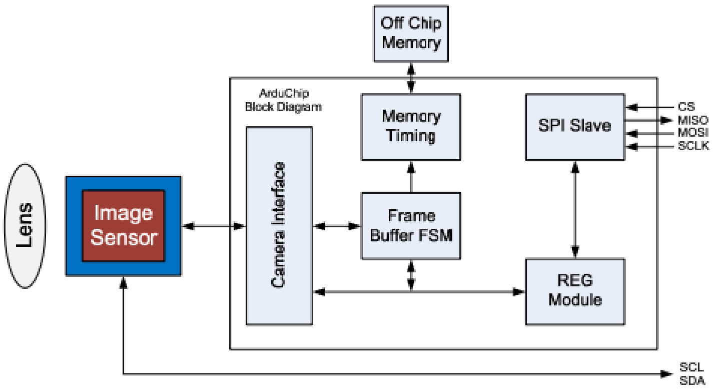

Figure 4.1: Camera Architecture of Arducam Mini OV2640 Camera Module

connected to the camera module through an I2C interface. Using the I2c interface it possible to set registers that control the functioning of the camera such as the output format, digital signal processing, etc. SPI interface is used to transfer the image data from the camera module to the Arduino. The Arduino upon receiving the image data either writes it to an SD card or sends it to the software on the PC through the USB connection.

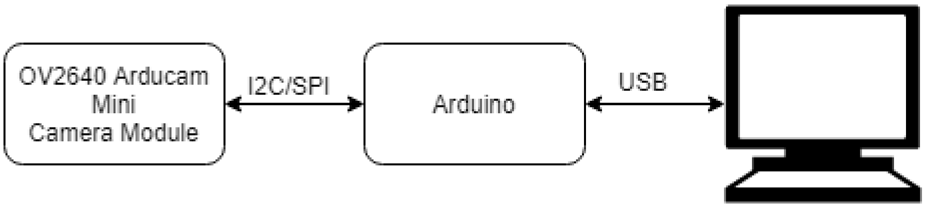

Figure 4.2: Implementation Setup

4.1.1 Exposure Control of OV2640

In order to do experiments, it was required to control the exposure of the camera. In the default driver that was provided by the vendor, the exposure was automatically set using the Automatic Exposure Control (AEC) feature in the sensor. So, a modification was needed in the driver software. Fortunately, the driver is open source and the there were libraries that could assist in setting the on-board registers through the I2C interface on the Arduino. First, let us have a look at how exposure control works in an OV2640 camera. All rolling shutter image sensors including OV2640 exposure the sensor one-line at a time i.e. pixels in the same line are exposed at the same time and different pixels in different lines are exposed at a different time. So, the minimum exposure time would be one line time and the maximum exposure time would be the frame time. This is illustrated in Figure 4.3.

By default the pixel clock is set at 36MHz. We can calculate the minimum line time using the following equation:

$$MinimumExposureTime = 1/PixelClock * PixelClockesperline$$

As shown in Figure 4.4, one line consists of 1922 pixel clocks(1600 for pixel data and 322 clocks of horizontal blanking). So the minimum exposure time would be 53.39μseconds and the maximum exposure time would be the frame time(multiply line time by 1200 + 44 lines of vertical blanking) which would be 66.63ms[3]. In order to control the exposure of the camera it is necessary to modify registers of address 4, 10, 13, 45. So, these registers were modified according the the required exposure time value. The driver software on the Arduino was modified to obtain different exposure times.

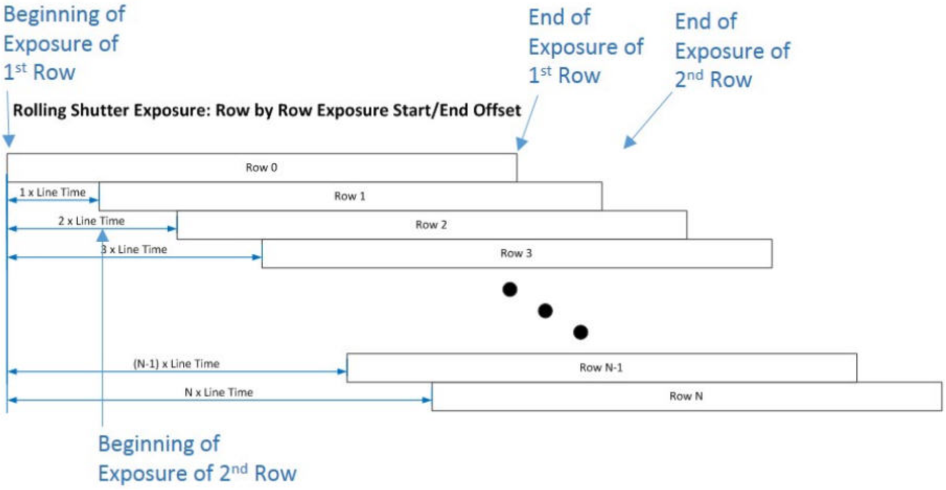
Beginning of Exposure of 1st Row
End of Exposure of 1st Row
End of Exposure of 2nd Row
Rolling Shutter Exposure: Row by Row Exposure Start/End Offset
Row 0
1 x Line Time
Row 1
2 x Line Time
Row 2
3 x Line Time
Row 3
(N-1) x Line Time
Row N-1
N x Line Time
Row N
Beginning of Exposure of 2nd Row

Figure 4.3: Rolling Shutter Operation on OV2640[3]

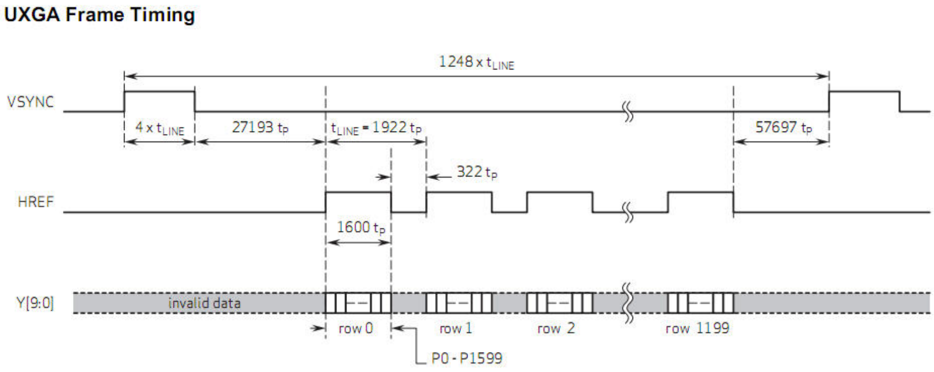

Figure 4.4: Shutter Timing Diagram of OV2640[3]

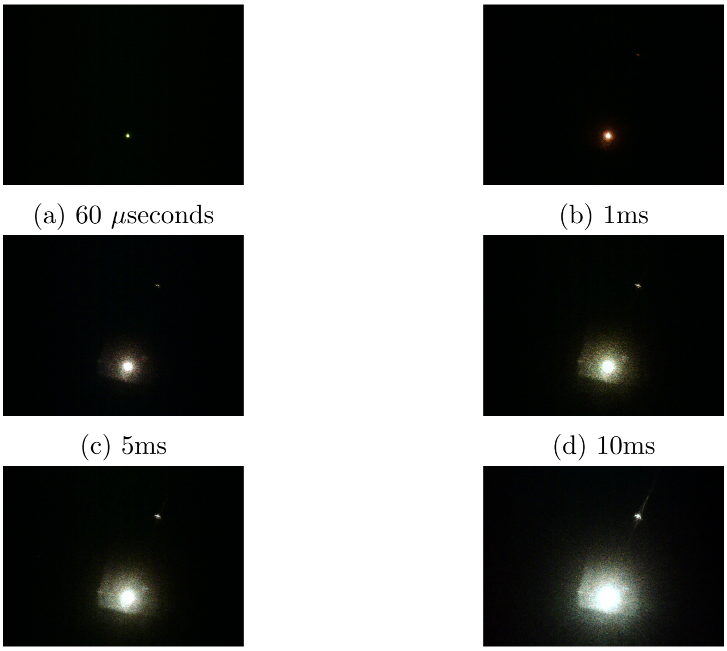

(a) 60 μseconds

(b) 1ms

(c) 5ms

(d) 10ms

(e) 20ms

(f) 60ms

Figure 4.5: Images of a laser beam caught in different exposure times(with lens)

4.2 Testing of Acceptance Cone of Sensor

4.2.1 Experimental Setup

Figure 4.6 shows the experimental setup that was made to measure the acceptance cone of the sensor. A collimated laser beam was reflected off a mirror and it is passed through a pinhole. The pinhole was used because a diverged wave did not provide much information about the distribution of energy of the signal. Hence, a pinhole was introduced to focus the beam onto a reduced area on the sensor. The difference in measurements with and without pinhole is shown in Figure 4.7.

The pinhole cannot be used to measure the acceptance cone of the sensor because the waveform from the pinhole is a combination of different plane waves of different frequencies. Hence, the measurement was done without a pinhole. In order to measure the acceptance cone of the sensor, it is necessary to identify a portion of the image that can be taken as a reference to plot the variation in the signal measurement. It was assumed that the maximum point in the image can be taken as the signal. Since there was too much variation in the intensities measured, it was decided that we would average the 10 images in each angular position to reduce the signal noise. The maximum value in the image was taken and normalized and the measure-

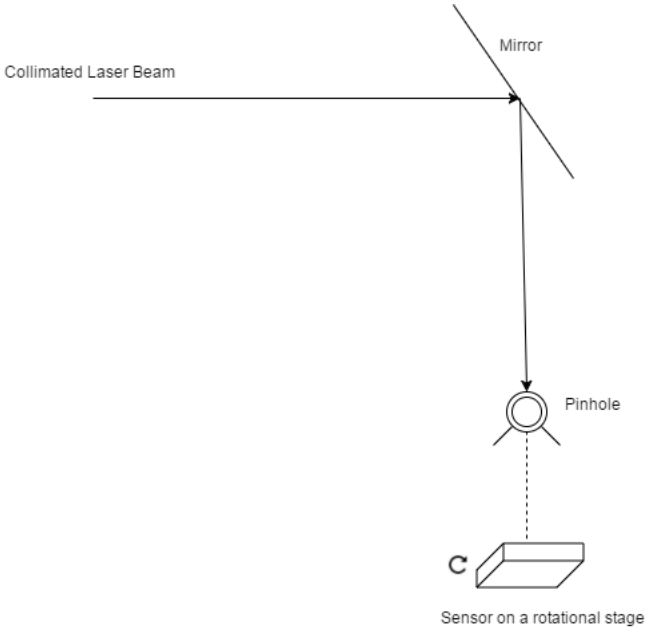

Figure 4.6: Experimental Setup for detection of acceptance cone

(a) Image without pinhole

(b) Image with pinhole

Figure 4.7: Images of a laser beam caught with and without pinhole

ments were repeated from -45 to +45 for 10 sets. The same image readings were used for finding out the response of different color channels(RGB). This experiment took a period of two weeks to complete. The exposure value was chosen such that the output does not saturate(does not reach 255) for any value in the image(See Figure 4.8). The maximum value in the image versus the angle is plotted. The ideal exposure value would be the one in which the the signal does not saturate and there is still some room for additional signals. This is also indicated in Figure 4.8.

The obtained response curves for each channel are shown in Figure 4.9, 4.10, 4.11. The normalized signal values are plotted with the standard deviation obtained for each angle are indicated with the use of an error bar. The best obtained curve fit is also plotted.

The initial observations from the results obtained are:

- There seems to be a very large standard deviation for each angle.

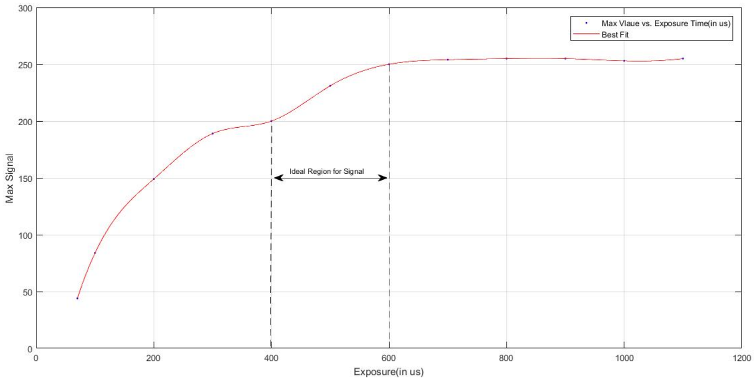

Figure 4.8: Response for different Exposure values in microseconds

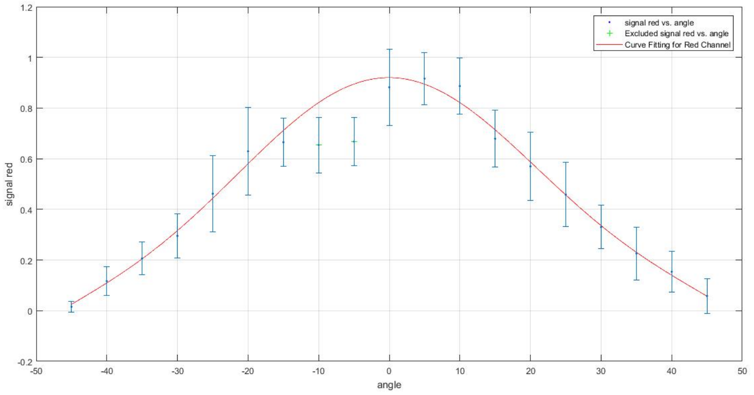

Figure 4.9: Response for Red Channel in Initial Experiment

- There seems to very sharp outliers at -5 and -10 degrees which is an highly unexpected behaviour.

These two observations point to experimental error. The error in the experimental results could be due to the following reasons:

- **Error introduced due to translation of the rotational stage :** In order to make sure that the beam always hits the stage is translated if the beam does not hit due to translation of the sensor away from the beam. This introduces an additional angular error which is not taken into account in the initial experiment. So, the stage was calibrated using the pinhole. If the sensor is exactly at the center of rotation of the rotational stage, the laser beam must always hit the same position of the sensor no matter what the rotational angle may be. The position of the sensor on the rotational stage was calibrated such that the

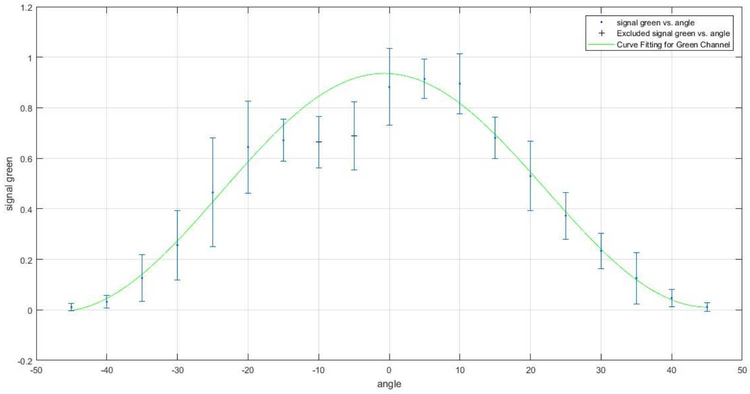

Figure 4.10: Response for Green Channel in Initial Experiment

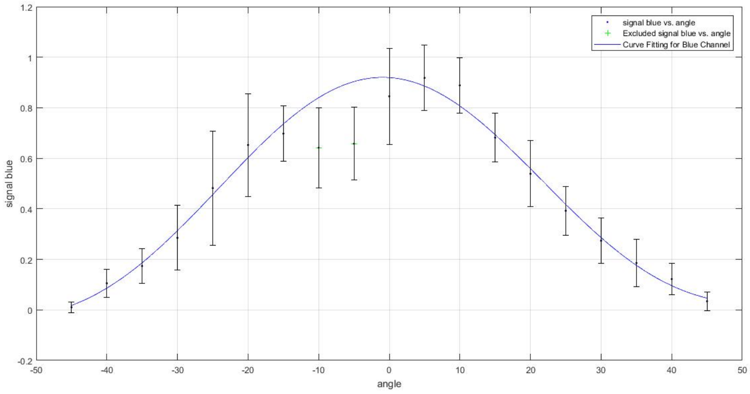

Figure 4.11: Response for Blue Channel in Initial Experiment

signal(image with pinhole) obtained always remained at the center of the sensor.

- **Improper Reference Signal from Image :** At times, it was observed that the maximum point in the image occurs at different and unexpected points that are outside the beam. This also leads to different parts of the signal being measured each time. The outliers in the results could also mean that. An example average image in which the maximum is obtained at the end of the beam is shown in Figure 4.12. The point from where the signal is obtained is marked using a yellow star in the Figure 4.12.

- **Large Variation on intensity of output image :** It was noticed that there was a huge variation in intensity for subsequent measurements at the very subsequent instants. This variation in the output

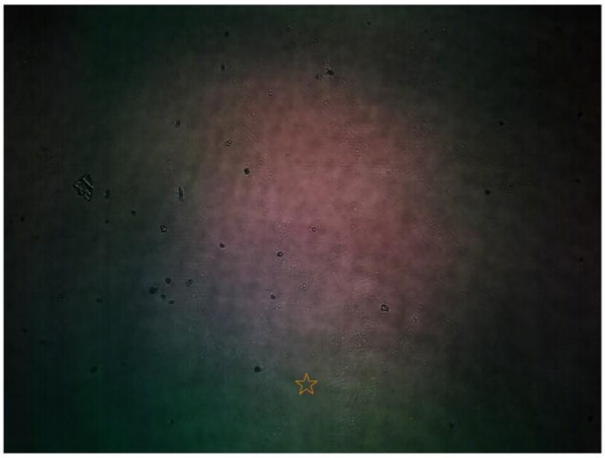

Figure 4.12: Improper Reference Point for Signal

is the cause of the large standard deviation in the result. Initially, I thought that this could be due to a relatively low exposure time(as lower exposure could lead to more output noise) or due to the variation of intensity of laser beam. Increasing the exposure time did give lower variations but the problem was traced to the automatic gain control in the OV2640 image sensor. The amplifier gain of each pixel was adjusted automatically and this led to different intensities in subsequent readings. After this feature was turned off by modifying the driver software using I2C, it seemed that the variation in the output was no longer there.

- **Unexpected Colors in the output image :** An unexpected feature in the image is seen in each measurement. The unexpected feature is the presence of green and blue colors of the laser beam. Since the laser beam is red with almost constant wavelength in the red visible light region, the output of green is unexpected. This was very strange and upon studying the sensor, it seemed that the sensor had an automatic white balance(AWB) feature of OV2640. This white balance feature assumes a "gray" world(wherein the average of all colors in the world is gray)[13] which is not true in our case. The difference in the output is with and without AWB is shown in Figure 4.13. Even after this adjustment, there seems to be a slight tinge of green at negative angles where the beam seems to "dim" out. Even after trying out a variation of different settings this green could not be eliminated and could be due to Black Level Calibration in the sensor. The function of Black

Level Calibration (BLC) is to product accurate color in the dark area of picture. There is no mention of how to turn off this feature in the data sheet or the application notes of this sensor. The vendor of the camera did not provide any information on how to turn off this feature. Hence, it was assumed that the sensor does not make any modifications to the red channel in angles where the signal "dims" out.

(a) Image with AWB

(b) Image without AWB

Figure 4.13: Images of a laser beam caught with and without pinhole

4.2.2 Improved experiment

As mentioned in the previous experiment, the stage was calibrated such that the sensor remains at the center of rotation of the rotational stage. The reference signal was chosen such that the same point of the beam is always measured. In order to make sure that the same point of the beam is measured with and without pinhole, the coordinate of the central diffraction pattern is stored for different angular positions for -45 to +45 and the reference signal is taken from this point. In order to detect the central region in the output, a function called `imfindcircles` is used[2]. This function finds circles in an image using using circular Hough transform. The readings for a specific angle are averaged and a logarithmic function is applied which is then passed to the `imfindcircles` function to detect the brightest possible circle with a radius of 3 pixels(This value was tuned such that the central portion is detected with 100 percent accuracy). The detection process using this this method provided 100 percent accuracy for detection of the center of the central fringe pattern coordinate. This is illustrated in Figure 4.14. The Automatic gain controls and Automatic White balance features of the CMOS sensors were turned off by using suitable register settings mentioned in [12]. The Arduino was programmed to set the register values using I2C. The exposure was set at 500μs based on the exposure graph mentioned in the previous section.

In the first step of the experiment, the rotational stage is rotated from -45 to +45 degrees with pinhole, and the coordinates of the central diffraction pattern is stored in a variable. In the second step of the experiment, the pinhole is removed and the signal is taken for different angle from the

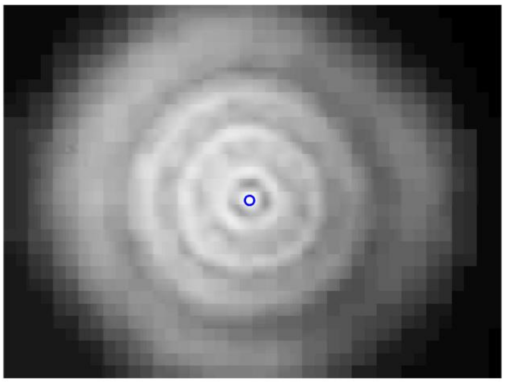

Figure 4.14: Coordinate Detection for central region signal detection

coordinates mentioned in the previous step. After this, the signal is taken with different offset(from the central diffraction pattern) in the X-direction to make sure that all the pixels behave in the same manner. The graphs for 100 different pixel positions from the central position is shown in Figure 4.15. From this graph,it can be seen that all the pixels in the same line exhibit the same behaviour. The experiment is repeated for 10 times and the

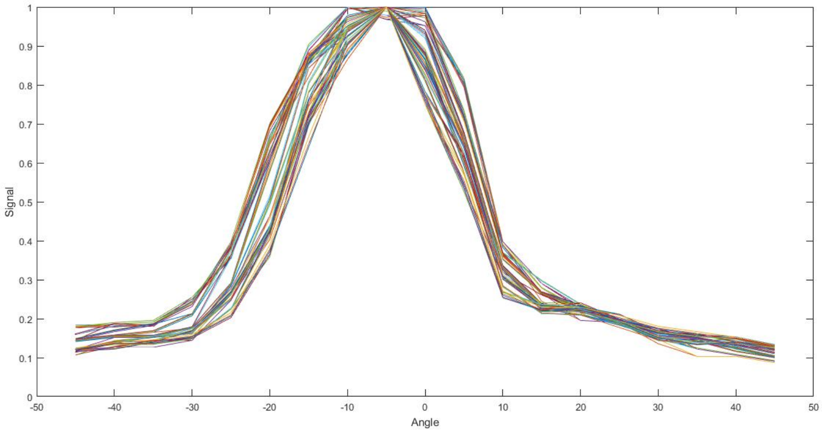

Figure 4.15: Response for 100 different offset pixel positions from central diffraction pattern

response is plotted only for the red channel as we have only red frequency light hitting the sensor beam. The final result after solving the problems mentioned in the previous section is shown in Figure 4.16. The standard

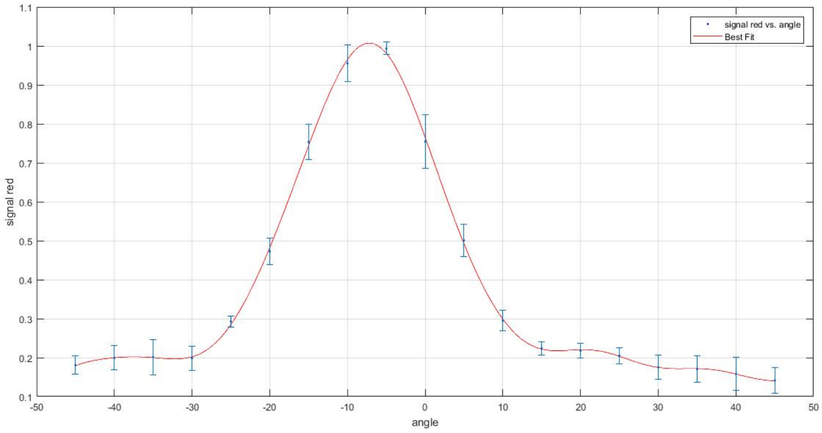

Figure 4.16: Red Channel Response for Different Data Sets

deviation of the data has also reduced as shown in the Table **??**. It can be seen that the standard deviation has reduced for all the angular position thereby increasing the experimental accuracy and repeatability. There is less overlap in the subsequent angles and no points for excluded in the curve fitting process. The maximum standard deviation has reduced from 16 percent for angular position -20 to 6 percent for angular position 0. The peak of the curve is shifted towards -5 degrees because the maximum position of the laser beam occurs at -5 degree position of the rotational beam. This data needs to be incorporated into the simulation to see the effect of the acceptance cone of the sensor on the image reconstruction. This will be discussed in the subsequent section.

4.3 Spatial Light Modulators

A spatial light modulator (SLM) is an object that imposes some form of spatially varying modulation on a beam of light[4].SLMs can be controlled by computer controlled software and it would be possible to generate patterns on the SLM that could modulate phase or the intensity of the beam or both simultaneously. An advantage of using an SLM over designing a lithographic mask is that it would be possible to test out different designs of masks quickly in order to find out an optimal mask configuration that would be suitable to our setup. In our design of the lensless imager, it must be possible to block and allow light in a certain binary pattern. A transmissive SLM would suit the purpose of simulating different mask patterns. For this purpose, a holoeye LC2012 SLM was used

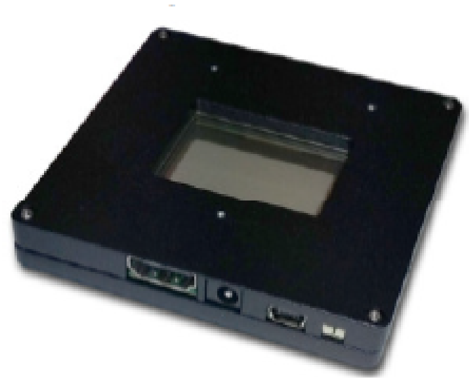

Figure 4.17: HoloEye LC2012 SLM

Chapter 5

Experimentation and Validation

INTRODUCTION TEXT TO THIS CHAPTER IN WHICH ALL SECTIONS ARE DESCRIBED ROUGHLY (1 SENTENCE EACH).

This chapter describes the ... In Section 5.1, examples are given of how to use tables and figures in MSc theses.

5.1 SECTION TITLE

Every caption of a table (or figure) should start with a capital letter, and should end with a period. References to tables are given with a capital letter for table, as in "(see Table 5.1)" or "in Table 5.1, ...".

left aligned	centred	right aligned
12	34	56

Table 5.1: Complete sentence describing the tabular data.

References to figures are given with a capital letter for figure, as in "(see Figure 5.1)" or "in Figure 5.1, ...".

[?] [?]

Figure 5.1: Complete sentence describing the figure thoroughly.

Chapter 6

Conclusions and Future Work

6.1 Conclusions

TODO CONCLUSIONS

6.2 Future Work

TODO FUTURE WORK

Bibliography

[1] Imaging geometries. http://www.its.caltech.edu/~ee157/lecture_note/Imaging%20geometries.pdf. Accessed: 2017-05-20.

[2] imfindcircles. https://nl.mathworks.com/help/images/ref/imfindcircles.html. Accessed: 2017-08-17.

[3] Manual exposure for ov2640. http://www.arducam.com/manual-exposure-ov2640/. Accessed: 2017-06-28.

[4] Spatial light modulators. https://en.wikipedia.org/wiki/Spatial_light_modulator. Accessed: 2017-06-29.

[5] V. Boominathan, J. K. Adams, M. S. Asif, B. W. Avants, J. T. Robinson, R. G. Baraniuk, A. C. Sankaranarayanan, and A. Veeraraghavan. Lensless imaging: A computational renaissance. *IEEE Signal Processing Magazine*, 33(5):23–35, Sept 2016.

[6] T. M. Cannon and E. E. Fenimore. Coded aperture imaging: Many holes make light work. *Optical Engineering*, 19(3):193283–193283–, 1980.

[7] Michael J. DeWeert and Brian P. Farm. Lensless coded-aperture imaging with separable doubly-toeplitz masks. *Optical Engineering*, 54(2):023102, 2015.

[8] Irfan Essa. Computational Photography Udacity Course. https://classroom.udacity.com/courses/ud955.

[9] A. El Gamal and H. Eltoukhy. Cmos image sensors. *IEEE Circuits and Devices Magazine*, 21(3):6–20, May 2005.

[10] Ir. A. Kamp. Instruments and their constituents. Space Instrumentation Engineering Lecture Notes, 2017.

[11] K. Khurshid, R. Mahmood, and Q. ul Islam. A survey of camera modules for cubesats - design of imaging payload of icube-1. In *2013 6th International Conference on Recent Advances in Space Technologies (RAST)*, pages 875–879, June 2013.

[12] Omnivision Technologies. *Preliminary Data Sheet*, 2 2006. V 1.6.

[13] Omnivision Technologies. *Software Application Notes*, 1 2008. V 1.04.